ACS APPLIED MATERIALS & INTERFACES

Research Article

www.acsami.org

Gold-Nanoparticles-Modified Cellulose Membrane Coupled with Laser Desorption/Ionization Mass Spectrometry for Detection of Iodide in Urine

Yu-Jia Li,[†] Yu-Ting Tseng,[†] Binesh Unnikrishnan,[†] and Chih-Ching Huang*[,†,‡,§]

[†]Institute of Bioscience and Biotechnology and [‡]Center of Excellence for the Oceans, National Taiwan Ocean University, Keelung, 20224, Taiwan

[§]School of Pharmacy, College of Pharmacy, Kaohsiung Medical University, Kaohsiung, 80708, Taiwan

Supporting Information

ABSTRACT: We report an efficient method for the determination of iodide (I^-) ions by using gold–iodide hybrid cluster ions on gold nanoparticles (Au NPs) modified mixed cellulose ester membrane (Au NPs-MCEM) by pulsed laser desorption/ionization mass spectrometry (LDI-MS). When I^- ions were deposited and concentrated on the surfaces of Au NPs (32 nm) via strong Au^+–I^- interaction on the MECM, the Au NPs-MCEM was observed to function as an efficient surface-assisted LDI substrate with very low background noise. When pulsed laser radiation (355 nm) was applied, I^- binding to Au NPs ions induced the enhancement of the desorption and ionization efficiency of gold–iodide hybrid cluster ions from the Au NPs surfaces. The reproducibility of the probe for both shot-to-shot and sample-to-sample (both less than 10%) ion production was also improved by the homogeneous nature of the substrate surface. Thus, it allows the accurate and precise quantification of I^- ions in high-salinity real samples (i.e., edible salt samples and urine) at the nanomolar range. This novel LDI-MS approach provides a simple route for the high-speed analysis of I^- ions with high sensitivity and selectivity in real biological samples.

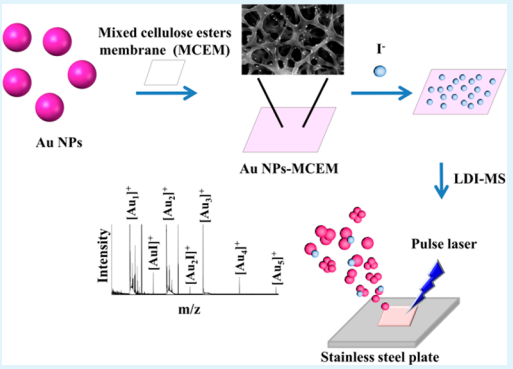

KEYWORDS: *mass spectrometry, gold nanoparticles, cellulose membrane, laser desorption/ionization, iodide, urine*

INTRODUCTION

Iodine is one of the micronutrients that are essential for human growth and metabolism.[1−3] In the human body, the thyroid gland produces thyroid hormones such as triiodothyronine and thyroxine using iodine and it helps in controlling many metabolic activities.[1,4] Also, in mammals, the dietary iodide is effectively utilized by two important thyroid proteins, sodium/iodide symporter and iodotyrosinedeiodinase.[1,4] Deficiency of dietary iodine or abnormal metabolism of iodine may cause goiter, hypothyroidism, and hyperthyroidism. In extreme conditions it may lead to developmental defects; thus, an iodine intake of 150 μg/day is recommended.[1−3] In urine, greater than 90% of total iodine is present as iodide (I^-).[5] Therefore, the determination of urinary I^- concentration is valuable for epidemiological studies of iodine supplementation, particularly in diagnosing and controlling iodine deficiency.[6−9] According to the World Health Organization, if the median urinary iodine concentration is less than 100 μg/L (approximately 0.8×10^{-6} M) in a population, it is considered to be iodine deficient.[10] In addition, measuring the I^- concentration in urine is useful for the diagnosis of transient thyroid dysfunction and iodine-induced hyperhidrosis.[7,11] Patients with iodine-induced hyperthyrosis have 10- to 100-fold more urinary iodide than healthy patients.[1−3]

Various methods based on different principles have been proposed to detect and determine the I^- concentration. The most widely practiced spectrophotometric method was the Sandell–Kolthoff reaction, in which yellow Ce^{4+} is reduced to colorless Ce^{3+} by As^{3+} in the presence of iodide.[12] Nowadays, several other methods such as electrochemical detection, gas chromatography, electrostatic ion chromatography, liquid chromatography, capillary electrophoresis, and optical spectrometry have been developed with good selectivity and sensitivity.[13−23] Earlier reports of iodide determination by ion chromatography using tubular ion-selective electrode show a linear range of 5–400 μg/L and a limit of detection of 1.47 μg/L.[19] Nguyen et al. reported the iodide determination in urine by ion-pair reversed-phase HPLC and pulsed amperometric method with a dynamic range of 20–250 μg/L; however, it is a slightly time-consuming process because of the two pretreatment steps involved.[20] Hu et al. used ion chromatography for the determination of fluorine and iodine in urine simultaneously, after decomposition in alkali and pretreatment using an electrochemical oxidation–neutralization device.[21]

Received: July 1, 2013
Accepted: August 26, 2013
Published: August 26, 2013

   dx.doi.org/10.1021/am4025824 | ACS Appl. Mater. Interfaces 2013, 5, 9161−9166

The inductively coupled plasma mass spectrometry (ICP-MS) technique can detect iodide with good sensitivity but needs an internal standard to reduce matrix effects.[22] Ion chromatography coupled with electrospray ionization tandem mass spectrometry is also a useful tool for the sensitive and selective quantification of nitrate, thiocyanate, perchlorate, and iodide in urine.[23] Although the sensitivity of some methods is high, these methods require complicated, multistep sample preparation and only a few reports are available for the I^- determination in complicated biological samples mainly because of problems associated with matrix interferences.

Recently, many optical-based probes have been developed using small molecules and nanoparticles (NPs) for the sensing of I^- ions,[24−33] Li et al. demonstrated I^- detection in urine by a chemiluminescence method with a limit of detection of 5×10^{-8} M.[32] However, common interferrants present in urine such as catechol, hydroquinone, pyrogallic acid, tannic acid, gallic acid, etc. show interference. In this method, the urine samples are baked at 600 °C to avoid the interference. Recently, a highly selective method that employs the aggregation of Au NPs has been reported by Zhou et al. for the detection of I^-, with a linear response from 4×10^{-8} to 4×10^{-6} M.[33] The assay fabrication includes the use of Hg and ssDNA. The low sensitivity and matrix interference of these NPs-based probes limit their practical applications in real samples. Therefore, the development of simple techniques for the determination of I^- in both biological (e.g., urine) and environmental samples has become increasingly important.

Gold nanoparticles (Au NPs) can act as selective probes as well as matrixes for the surface-assisted laser desorption/ionization mass spectrometry (SALDI-MS) analyses of metal ions and various other organic molecules such as aminothiols, peptides, proteins, oligonucleotides, and carbohydrates.[34] Regardless of the advantages and encouraging results obtained with Au NPs, due to efficient thermally driven energy transfer, LDI is accompanied by the production of a certain amount of Au cluster ions.[35] Consequently, the signals of the analytes are suppressed, forming complicated mass spectra, and thus, this lowers the analytical sensitivity. Moreover, Au NPs form an inhomogeneous distribution on the target plate when Au NP solution is dropped and air-dried at room temperature. This inhomogenerous distribution also results in poor sample-to-sample reproducibility.[34] This study develops a simple LDI-MS-based sensor using Au NPs-modified mixed cellulose ester membrane (Au NPs-MCEM) for the rapid quantification of I^- ions in urine. Instead of monitoring I^- ions by MS, the analysis utilizes the strongly efficient desorption and ionization of gold−iodide hybrid cluster ions ($[AuI]^+$) by LDI-MS to detect I^- ions (Scheme 1). The Au NPs-MCEM nanocomposite probe displayed high sensitivity and selectivity toward I^-. The use of the homogeneous Au NPs-MCEM nanomembrane can provide high reproducibility (<10%) of hybrid cluster ions. Also, we demonstrate the practical application of this approach for the determination of I^- ions in human urine samples.

Scheme 1. Schematic Representation of the Preparation of the Gold-Nanoparticle-Modified Mixed Cellulose Ester Membrane (Au NPs-MCEM) Substrate and Its Application for the Determination of I^- Ions via Laser Desorption Ionization Mass Spectrometry (LDI-MS)

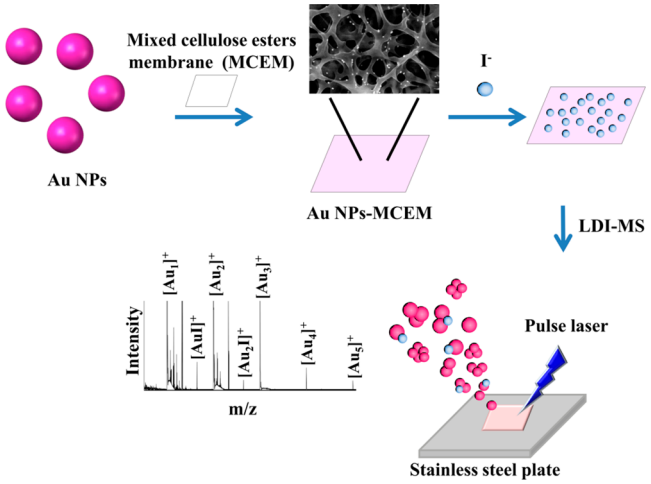

MATERIALS AND METHODS

Chemicals. Trisodium citrate, phosphoric acid, and citric acid monohydrate were purchased from Aldrich (Milwaukee, WI). MCEMs (pore sizes of 0.10, 0.45, and 5.0 μm) and cellulose acetate membranes (pore size of 0.45 μm) were purchased from Advantec (Toyo Roshi Kaisha, Japan). Amersham Hybond-C Extra nitrocellulose membranes (pore sizes of 0.10 and 0.45 μm) were purchased from GE Healthcare Bioscience (Buckinghamshire, U.K.). Polyvinylidene fluoride membranes (pore size of 0.45 μm) was purchased from Pall (Pall Corporation, U.K.). Hydrogen tetrachloroaurate (III) trihydrate ($HAuCl_4$), sodium thiosulfate pentahydrate ($Na_2S_2O_8{\cdot}5H_2O$), and hydrogen peroxide (H_2O_2) were obtained from Acros (Geel, Belgium). NaCN, NaSCN, CH_3COONa, NaBr, $NaBrO_3$, KCl, $NaClO_4$, Na_2CO_3, KI, KIO_3, Na_2S, and Na_2SO_4 were obtained from Alfa Aesar (Ward Hill, MA). Phosphate buffer solution (0.1 M, pH 7) was prepared with Na_2HPO_4 and $NaH_2PO_4{\cdot}H_2O$ obtained from J. T. Baker (Phillipsburg, NJ, USA). Milli-Q ultrapure water (Millipore, Billerica, MA) was used in all experiments.

Preparation of Au NPs and Fabrication of Au NPs-MCEM. For the preparation of 32 nm Au NPs, Au NP solution was synthesized as mentioned in our previous report.[36] An amount of 0.5 mL of 1% trisodium citrate solution was rapidly added to 50 mL of 0.01% $HAuCl_4$ solution and boiled in a flask equipped with reflux condenser for 8 min, and the color of the solution changed to pink indicating the formation of 32 nm Au NPs (32 ± 6 nm). The concentration of the 32 nm Au NPs was 2.8×10^{-10} M. A sodium citrate buffer (2.5×10^{-3} M, pH 5.8) solution was prepared by mixing 0.1 M citric acid and 0.1 M sodium citrate solution. An MCEM with a size of 0.5 cm (length) × 0.5 cm (width) was used for the preparation of the Au NPs-MCEM substrate. Forty MCEMs were immersed in the Au NP (32 nm) solution (3.0×10^{-11} M, 20 mL) with a 2.5×10^{-3} M citrate solution (pH 5.8) in a 20 mL screw vial and incubated for 2 h. The Au NPs-modified MCEM (Au NPs-MCEM) was gently washed with 20 mL of deionzed water for 30 s and dried in air for 1 h at room temperature. For conducting of the color analysis of the prepared membrane, it was scanned using an Epson desktop scanner (Epson Perfection 1660 photoscanner) and the color intensity of pixels was analyzed (red, green, and blue) using Image J computer program.

Detecting I^- Ions Using the Au NPs-MCEM. The as-prepared Au NPs-MCEM was immersed in 1 mL aliquots of 5 mM phosphate buffer solution (pH 7.0) containing I^- ions ($(0-1.0) \times 10^{-5}$ M), and the mixture was kept for 1 h at room temperature to attain equilibrium. The membranes were gently washed with 5 mL of deionized water for 30 s and dried in air at room temperature and then attached onto a MALDI plate using an adhesive polyimide film tape. Mass spectrometry experiments were performed in the reflectron positive-ion mode using an AutoflexIII MALDI time-of-flight (TOF) mass spectrometer (Bruker Daltonics, Bremen, Germany). The samples were irradiated using pulsed laser irradiation (355 nm Nd:YAG, 100 Hz, 102.5 W cm^{-2}, pulse width 6 ns). A delayed extraction period of 20 ns was set to energetically stabilize the positively charged ions produced during LDI, and then the ions were

accelerated through the TOF chamber in the reflection mode before entering the mass analyzer. The accelerating voltages were applied in the range from +20 to −20 kV. The instruments were calibrated before recording the mass spectra, using Au clusters ($[Au_x]^+$, x = 1−5). To accumulate signals, 600 pulsed laser shots with a laser fluence of 102.5 W cm^{-2} were applied to five random positions on the MALDI target plate.

Analysis of I$^-$ in Real Samples. A urine sample to be used for testing urinary iodide was collected from each of five healthy humans (20−30 years old) in the early morning because the metabolite level in the urine may vary during the day. Insoluble materials were removed by centrifugation (RCF 3000g, 30 min) and filtered through a 0.2 μm membrane. Then the filtered urine was diluted 25 times with 5.0 × 10^{-3} M phosphate buffer (pH 7.0) containing 0.5 M H_2O_2 and 5.0 × 10^{-3} M ascorbic acid and divided into 1 mL aliquots. Then the samples were separately analyzed by ICP-MS and LDI-MS with the Au NPs-MCEM substrate. Edible salt samples with different KIO_3 levels were purchased from Taiwan Salt Industrial Corporation (Miaoli, Taiwan). For the analysis, an edible salt solution of 0.3 g/mL was prepared in deionized water. Then the IO_3^- in the salt solution was reduced to I$^-$ by treating it with 5.0 × 10^{-3} M ascorbic acid for 10 min. From this solution, aliquots of the 30-fold-diluted edible salt samples (1000 μL) containing 5.0 × 10^{-3} M ascorbic acid and 5.0 × 10^{-3} M phosphate buffer (pH 7.0) were prepared. Then the samples were separately analyzed by ICP-MS and LDI-MS using the Au NPs-MCEM substrate.

RESULTS AND DISCUSSION

LDI-MS-Based Sensor for I$^-$ Ions. Scheme 1 depicts the procedure for the fabrication of Au NPs-MCEM and its application for LDI-MS for the detection of I$^-$ ions. MCEMs are made of cellulose nitrate (80%) and cellulose acetate (20%), widely used in filters for sterilizing biological fluids, microbiology, contamination analysis, and air monitoring.[37−40] The nitrate dipole on the MCEM helps the binding of Au NPs on it almost immediately through electrostatic interaction as well as through the hydrophobic (interfacial) interaction. The leaching of Au NPs from MCEM was less than 1% after Au NPs-MCEM was incubated in 5.0 × 10^{-3} M sodium phosphate solution (pH 7.0) for 48 h. The incompletely reduced Au NPs surface possesses Au^+ shell with positive charges, while the core Au atoms of the NP remain as Au^0. The I$^-$ ions bind preferentially to Au{111} by strong Au^+−I$^-$ interactions (cohesive energy of 360 kJ mol^{-1}),[41] increasing the concentration of I$^-$ ions on the membrane. Figure 1 shows the LDI mass spectra obtained for the MCEM (pore size of 0.1 μm) and Au NPs (size ∼32 nm) MCEM. A flat and very clean mass spectrum was observed for the blank MCEM (Figure 1A). Upon pulsed laser irradiation (355 nm Nd:YAG, 100 Hz, 102.5 W cm^{-2}, pulse width 6 ns) of the Au NPs-MCEM (Figure 1B), the absorption of the laser energy by the Au NPs induces the desorption and ionization of the surface atoms, producing cationic clusters ($[Au_n]^+$, n = 1−5). In contrast to Au NPs on a stainless steel 384-well MALDI target plate (Figure S1 in the Supporting Information), the MS spectrum shows relatively few interference peaks by using Au NPs-MCEM as the matrix, presumably because cellulose nitrate and cellulose acetate effectively bind with the interfering cationic molecules because of their negatively charged sites. This binding could limit or eliminate the interference from cationic molecules. During the nanosecond pulsed-laser excitation, the formation of Au cluster ions could happen by the fragmentation of Au NPs which might be favored by the photothermal surface evaporation mechanism.[42] The pulse width (τ_P) of the nanosecond laser pulse is longer than the relaxation times of Au NPs. For example, the phonon−phonon

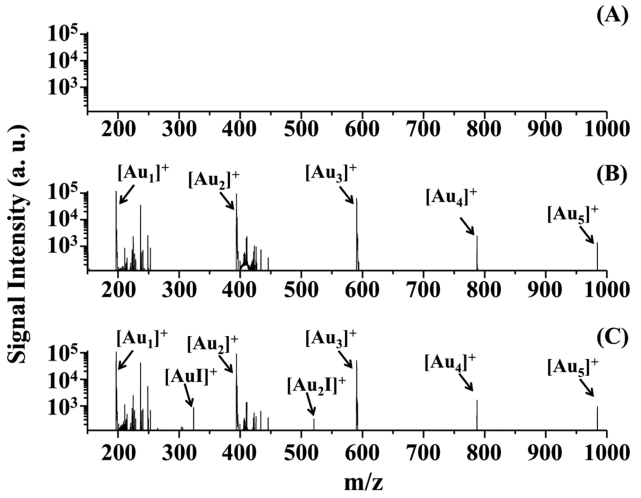

Figure 1. Mass spectra of (A) MCEM, (B) Au NPs-MCEM, and (C) Au NPs-MCEM in the presence of I$^-$ ions (1.0 × 10^{-7} M). The peaks at m/z = 196.97, 323.87, 393.93, 520.84, 590.90, 787.87, and 984.83 are assigned to $[Au_1]^+$, $[AuI]^+$, $[Au_2]^+$, $[Au_2I]^+$, $[Au_3]^+$, $[Au_4]^+$, and $[Au_5]^+$, respectively. To get good reproducibility and accumulate signals, 600 pulsed laser shots with a laser density of 102.5 W cm^{-2} were applied to five random positions on the MALDI target. Peak intensities are plotted in arbitrary units (a. u.).

relaxation time ($\tau_{ph\text{-}ph}$) and the electron−phonon relaxation time ($\tau_{e\text{-}ph}$) for Au NPs are 50−600 and 2−3 ps, respectively. As a result, the boiling temperature is easily reached, whereas a fragmentation temperature that exceeds the Rayleigh instability limit is not.[43,44] The peak intensities of $[Au_4]^+$ and $[Au_5]^+$ cluster ions were much lower than those of the $[Au_{1-3}]^+$ ions, which can be explained by the fact that the yield (Y_n) of metallic clusters of n atoms is proportional to $n^{-\delta}$, where δ is related to the total sputter yield.[45]

The mass spectra were recorded for the Au NPs-MCEM as LDI substrate in the presence of 1.0 × 10^{-7} M I$^-$ ions (Figure 1C). The I$^-$ ions were detected at m/z = 323.87 for $[AuI]^+$ ions and m/z = 520.84 for $[Au_2I]^+$ ions. The I$^-$ ions attached to the surface of Au NPs is not to Au monoatoms; therefore, $[AuI]^+$ and $[Au_2I]^+$ cluster ions could probably be formed during the laser ablation. We did not do model reaction in this study. The delocalized valence electrons of formed $[AuI]^+$ and $[Au_2I]^+$ cluster ions are odd and even electrons, respectively. The higher signal intensity of $[AuI]^+$ is probably due to the relatively strong interaction of Au^+−I$^-$. We noted that the completion of electron shells for delocalized valence electrons of Au^+ in $[AuI]^+$ also contributes to their higher stability and therefore signal intensity.[45] The mass spectra under reflectron negative-ion mode did not produce any characteristic peaks of Au cluster anions $[I]^-$, $[AuI]^-$, and $[Au_2I]^-$ (data not shown) mainly because the pulsed laser irradiation could not produce negative Au cluster ions as efficiently as positive cluster ions. The homogeneous distribution of the Au NPs on the MCEM surface (Figure 2) provided the excellent shot-to-shot (<10%) and sample-to-sample (<10%) reproducibilities for the detection/production of the $[AuI]^+$ ion (Figure S2 in the Supporting Information). The UV−vis absorption spectra, scanning electron microscopy (SEM) image, and color analysis of Au NP-MCEMs reveal that the Au NPs are dispersed (no aggregation) and homogeneously adsorbed on the MCEM fibers (Figure 2). The high deposition of Au NPs on the highly porous MCEM (porosity of ∼65%) provides "crystallization

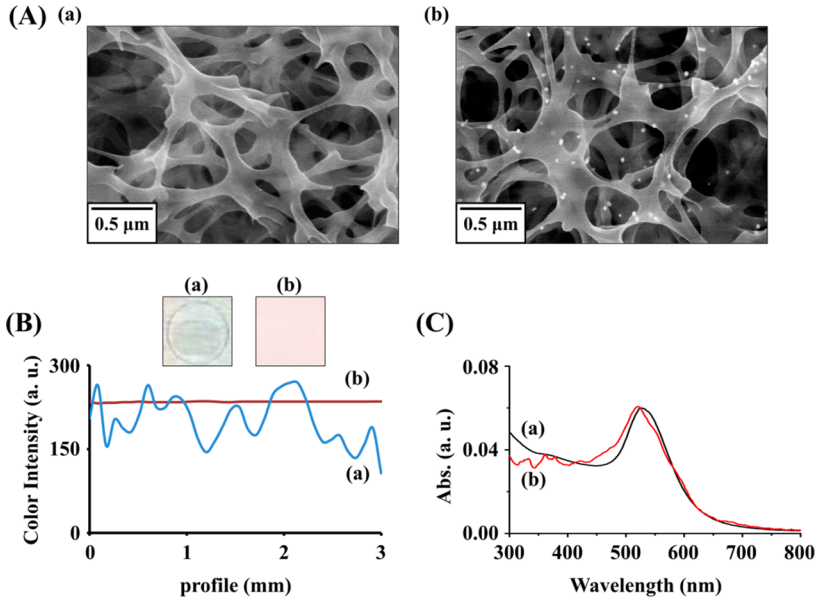

Figure 2. Scanning electron microscopy (SEM) images of (a) blank MCEM and (b) Au NPs-MCEM. (B) Color analyses of the (a) Au NPs (on a stainless-steel MALDI plate) and (b) Au NPs-MCEM, performed using the Image J computer program to compare their homogeneities. (C) UV–vis absorption spectra of the (a) Au NPs solution and the (b) Au NPs-MCEM substrate, recorded in transmission and reflection modes, respectively. The RSDs in (B) of profile analyses in (a) Au NPs on a stainless-steel MALDI plate and (b) Au NPs-MCEM were 20.8% and 0.6%, respectively.

networks" or "nucleation cores" for the formation of analyte/matrix cocrystals, implying that the MCEM acts as a crystallization moderator to create a dense network that generates a compositionally homogeneous layer of small sample/matrix cocrystals.[46−48]

Parameters for the Sensing of I^- Ions. We further studied the impact of composition and pore size of membranes on the detection of I^- ions by Au NPs-MCEM/LDI-MS via the monitoring of $[AuI]^+$ and $[Au_2I]^+$ ion signals (Figure S3 in the Supporting Information). The best detection performance was observed using I^- ions (1.0×10^{-7} M) in contact with an Au NPs-MCEM with a pore size of 0.1 μm. This matrix had the highest capacity for Au NPs loading, and its large negative charge eliminates interference from ionization and desorption during the LDI process. The surface melting and evaporation of Au NPs are highly dependent on the power density rather than the excitation wavelength of the laser.[42,45,49] The particle temperature was estimated to be $T = [(Q - \Delta H_{melt} - \Delta H_{vap})/C_p] + 293$ K by applying a simple thermodynamic model.[50] Here Q (J g^{-1}) represents the energy absorbed by a unit mass of gold through the irradiation of a single pulsed laser light, C_p is the specific heat capacity of Au (0.131 J g^{-1} K^{-1}), ΔH_{melt} is the enthalpy of melting (62.8 J g^{-1}), and ΔH_{vap} is the enthalpy of vaporization (1870 J g^{-1}). Figure S4 (Supporting Information) shows the signal intensities of the $[AuI]^+$ ions obtained from different laser power densities. At applied laser power densities below 96.4 W cm^{-2}, the boiling temperature (~3700 K) of the 32 nm Au NPs was not exceeded, and thus, the efficiency of fragmentation of the Au NPs was very low and led to a low signal of $[AuI]^+$. When the laser power density was increased from 96.4 to 102.5 W cm^{-2}, the signal intensity of the $[AuI]^+$ ions increased as sufficient energy was gained for desorption/ionization. Conversely, at higher laser power density (>102.5 W cm^{-2}), low signal intensity and complicated mass spectra were obtained, and it could be due to the complicated competitive desorption and ionization processes and gas phase reactions of the Au cluster ions with the desorbed molecules or ions.[48] Under the optimum laser power of 102.5 W cm^{-2} (Figure S4), our Au NPs-MCEM/LDI-MS system allowed the quantification of the I^- ions in sodium phosphate solution (pH 7.0) in the linear range from 1×10^{-9} to 1×10^{-5} M with regression coefficient $R^2 = 0.98$ in a plot between $[AuI]^+$ signal intensity and logarithm of I^- concentration. Beyond this concentration the peak intensity did not increase linearly, which could be due to the saturation of Au NPs surfaces with I^- ions. The LOD for I^- ions, at a signal-to-noise ratio of 3, was 5×10^{-10} M (~30 ppb). This LOD was comparable to that obtained from ICP-MS and is lower than those of optical and electrochemical sensors for I^- ions.[13−18,24−31]

Sensitivity and Selectivity of Au NPs-MCEM/LDI-MS System. We tested the selectivity of the Au NPs-MCEM/LDI-MS system for the detection of I^- in the presence of various anionic species (citrate, I^-, S^{2-}, ClO_4^-, IO_3^-, PO_4^{3-}, CH_3COO^-, Cl^-, SO_4^{2-}, Br^-, CO_3^{2-}, BrO_3^-, $S_2O_8^{2-}$, CN^-, and SCN^- ions). The Au NPs-MCEM substrate was immersed in buffer solution containing I^- or other anions for 1 h for the enrichment of I^- on the Au NPs. Figure 3 shows the plot of mass spectral signal intensities obtained for various anions (1.0×10^{-5} M each) and I^- (1.0×10^{-7} M), revealing that Au NPs-MCEM exhibits excellent selectivity toward I^- ions over other anions. The high selectivity of the Au NPs-MCEM for I^- ions results from the high binding affinity of Au^+ and I^- ions on the Au NPs surfaces.[41] It may also be attributed to the laser easily inducing the electron injection of chemisorption iodide on the particle's surface ($I^- + Au^+ \rightarrow AuI_{(adsorbed)} \rightarrow AuI^+_{(gas)} + e^-$),[51] which improves the ionization efficiency of $[AuI]^+$.

Analysis of I^- Ions in Real Samples. To evaluate the application of the developed probe for I^- detection in real samples, we tested the sensing strategy to determine the I^- content in three different edible salt samples. I^- determination in iodized salt is very important because it is widely used as an I^- supplement to overcome iodine deficiency in humans. The recommended iodine content in iodized salt is 46−77 ppm in

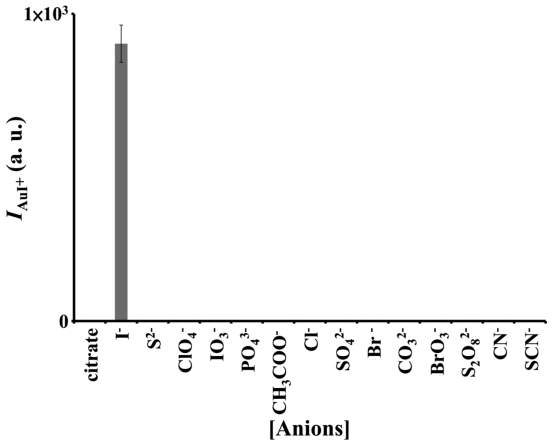

Figure 3. Selectivity of Au NPs-MCEM substrate as LDI-MS matrixes for different anions (1.0×10^{-7} M for I^- ions, 1.0×10^{-5} M for each of the other anions). Peak intensities of $[AuI]^+$ are plotted in arbitrary units (a.u.). Error bars represent the standard deviations from five repeated experiments. Other conditions were the same as those described in Figure 1.

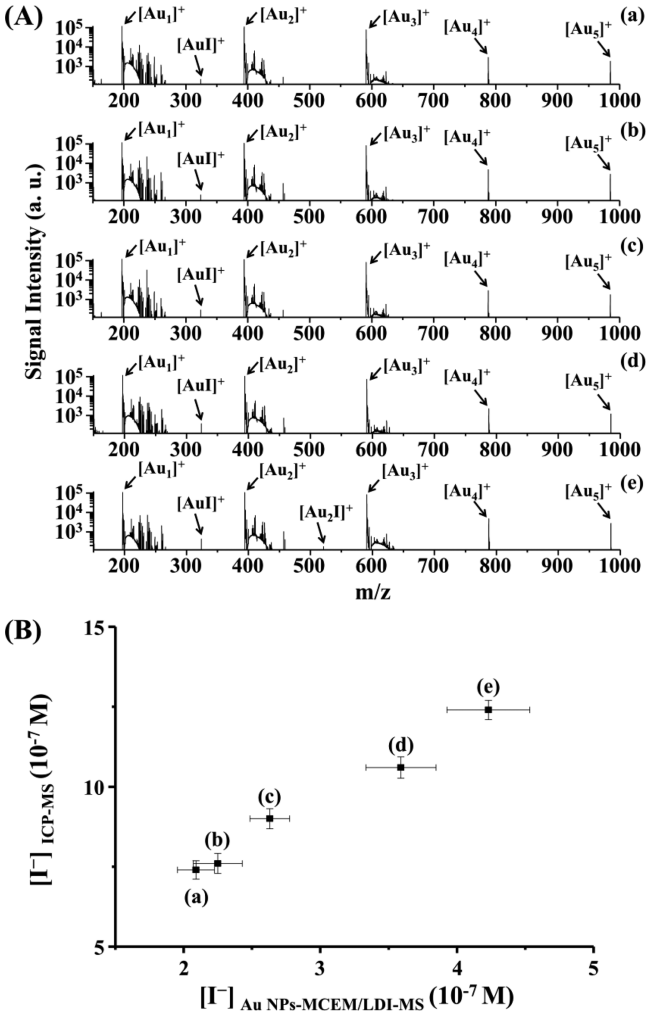

Figure 4. (A) Mass spectra recorded using Au NPs-MCEM for the detection of I^- in five (a–e) human urine samples (25-fold dilution). (B) Comparison between Au NPs-MCEM substrate as LDI-MS matrixes and ICP-MS for the determination of I^- in five human urine samples (a–e).

the U.S.[52,53] The three edible salt samples contain iodine in the form of IO_3^-. We pretreated the salts with 5.0×10^{-3} M ascorbic acid to reduce IO_3^- to I^- prior to analysis by Au NPs-MCEM/LDI-MS (Figure S5 in the Supporting Information). The I^- concentrations in the three edible salts were determined by the estimated standard curve in Figure S4 (curve C). Table 1 shows the *t*-test data for Au NPs-MCEM/LDI-MS system and ICP-MS measurements for the iodide ions that exhibit a 95% confidence interval and are in good agreement with the certified values.

We further used our Au NPs-MCEM/LDI-MS for the analysis of I^- ions in a complicated biological fluid such as human urine. We used the standard curve (curve C) in Figure S4 to determine the I^- concentration of five urine samples (parts a–e of Figure 4A). Figure 4B reveals a good linear correlation (r = 0.98) between the results from our Au NPs-MCEM/LDI-MS assay and ICP-MS over concentrations from 2.09×10^{-7} to 4.23×10^{-7} M, suggesting that the proposed probe can be applied for the determination of I^- ions in urine. The estimated values that our Au NPs-MCEM/LDI-MS provided for I^- ions in urine were lower than those obtained from the ICP-MS analysis, most likely because of matrix interference. In comparison with other NP-based sensor systems,[24−33] our developed label-free assay is relatively rapid, simple, and sensitive. Note that almost all other optical, chromatography, and electrochemical techniques are rarely applied to detect I^- ions in such a complicated sample as human urine.[13−18,24−33]

CONCLUSIONS

We demonstrated the Au NPs-MCEM as a novel LDI-MS substrate for I^- determination in high-salinity samples that are not under laboratory control (i.e., edible salt samples and urine). I^- ions were deposited on the Au NPs-MCEM to form a highly efficient LDI substrate with very less background noise. The binding of I^- ions to the Au NPs induced an enhancement of the desorption and ionization efficiency of gold–iodide hybrid cluster ions in the mass spectrum. Compared with conventional Au NPs-based LDI-MS methodologies, the Au NPs-MCEM probe was demonstrated to offer the ease of sample preparation, high desorption/ionization efficiency, and

Table 1. Determination of I^- Concentrations in Edible Salt Samples by Au NPs-MCEM/LDI-MS System

salt sample	certified range (ppm)	ICP-MS, mean ± SD (ppm, n = 5)	Au NPs-MCEM, mean ± SD (ppm, n = 5)	*t*-test between ICP-MS and Au NPs-MCEM[a]	consensus value (μM), 95% confidence interval[a]
A	0	ND[b]	ND[b]		
B	15.2	12.9 ± 2.5	15.6 ± 1.5	2.07	13.3–17.9
C	15.0–35.5	25.4 ± 3.2	29.3 ± 2.4	2.18	26.2–32.4

[a] *t*-test value is 2.31 at a 95% confidence level (degrees of freedom, 8). [b] Not detected.

dx.doi.org/10.1021/am4025824 | ACS Appl. Mater. Interfaces 2013, 5, 9161–9166

lower matrix interference in the mass spectrum. In addition the highly homogeneous characteristics of the Au NPs-MCEM surface improves the shot-to-shot and sample-to-sample reproducibility of the probe for ion production, thus facilitating high accuracy in measurements. This simple Au NPs-MCEM/LDI-MS system has promising potential as a probe for the detection of I^- in complicated biological samples.

■ ASSOCIATED CONTENT

Supporting Information

Figures S1−S5 displaying the comparison of mass spectra of Au NPs on steel plate, SEM images of Au NPs-MCEMs with different pore size, effect of laser density on the LDI-MS analysis, and the analyses of three edible salt samples. This material is available free of charge via the Internet at http://pubs.acs.org.

■ AUTHOR INFORMATION

Corresponding Author

*E-mail: huanging@ntou.edu.tw.

Notes

The authors declare no competing financial interest.

■ ACKNOWLEDGMENTS

This study was supported by the National Science Council of Taiwan under Contract NSC 101-2628-M-019-001-MY3.

■ REFERENCES

(1) Rokita, S. E.; Adler, J. M.; McTamney, P. M.; Watson, J. A., Jr. *Biochimie* **2010**, *92*, 1227−1235.
(2) Zimmermann, M. B. *Semin. Cell Dev. Biol.* **2011**, *22*, 645−652.
(3) Zimmermann, M. B.; Jooste, P. L.; Pandav, C. S. *Lancet* **2008**, *372*, 1251−1262.
(4) Hingorani, M.; Spitzweg, C.; Vassaux, G.; Newbold, K.; Melcher, A.; Pandha, H.; Vile, R.; Harrington, K. *Curr. Cancer Drug Targets* **2010**, *10*, 242−267.
(5) Vought, R. L.; London, W. T. *J. Clin. Endocrinol. Metab.* **1967**, *27*, 913−919.
(6) Konno, N.; Yuri, K.; Miura, K.; Kumagai, M.; Murakami, S. *J. Endocrinol.* **1993**, *40*, 163−169.
(7) Markou, K. B.; Georgopoulos, N. A.; Anastasiou, E.; Vlasopoulou, B.; Lazarou, N.; Vagenakis, G. A.; Sakellaropoulos, G. C.; Vagenakis, A. G.; Makri, M. *Thyroid* **2002**, *12*, 407−410.
(8) van der Merwe, D. E.; Henley, R.; Lane, G.; Field, R.; Frenneaux, M.; Dunstan, F.; McDowell, I. *Clin. Chem.* **2004**, *50*, 780−782.
(9) Zimmermann, M. B. *Endocr. Rev.* **2009**, *30*, 376−408.
(10) de Benoist, B.; Andersson, M.; Egli, I.; Takkouche, B.; Allen, H. *WHO Global Database on Iodine Deficiency*; World Health Organization: Geneva, 2004.
(11) Heinisch, M.; Kumnig, G.; Asböck, D.; Mikosch, P.; Gallowitsch, H.-J.; Kresnik, E.; Gomez, I.; Unterweger, O.; Lind, P. *Thyroid* **2002**, *12*, 809−814.
(12) Sandell, E. B.; Kolthoff, I. M. *Microchim. Acta* **1937**, *1*, 9−25.
(13) Ito, K.; Nomura, R.; Fujii, T.; Tanaka, M.; Tsumura, T.; Shibata, H.; Hirokawa, T. *Anal. Bioanal. Chem.* **2012**, *404*, 2513−2517.
(14) Malongo, T. K.; Patris, S.; Macours, P.; Cotton, F.; Nsangu, J.; Kauffmann, J.-M. *Talanta* **2008**, *76*, 540−547.
(15) Nguyen, B. D. Q.; Chernov'Yants, M. S.; Burykin, I. V. *Analyst* **2012**, *137*, 481−484.
(16) Pan, Y.; Zhang, X. *Water Res.* **2013**, *47*, 163−172.
(17) Rebary, B.; Paul, P.; Ghosh, P. K. *Food Chem.* **2010**, *123*, 529−534.
(18) Yokota, K.; Fukushi, K.; Ishio, N.; Sasayama, N.; Nakayama, Y.; Takeda, S.; Wakida, S.-I. *Electrophoresis* **2003**, *24*, 2244−2251.
(19) Almeida, A. A.; Jun, X.; Lima, J. L. F. C. *Mikrochim. Acta* **1997**, *127*, 55−60.
(20) Nguyen, V. T. P.; Piersoel, V.; El Mahi, T. *Talanta* **2012**, *99*, 532−537.
(21) Hu, K. K.; Huang, W. X.; Su, Y. H.; Hu, R. Z. *Chin. Chem. Lett.* **2009**, *20*, 1483−1486.
(22) Dyke, J. V.; Dasgupta, P. K.; Kirk, A. B. *Talanta* **2009**, *79*, 235−242.
(23) Valentín-Blasini, L.; Blount, B. C.; Delinsky, A. *J. Chromatogr., A* **2007**, *1155*, 40−46.
(24) Barman, S.; Sadhukhan, M. *J. Mater. Chem.* **2012**, *22*, 21832−21837.
(25) Chen, L.; Lu, W.; Wang, X.; Chen, L. *Sens. Actuators, B* **2013**, *182*, 482−488.
(26) Du, F.; Zeng, F.; Ming, Y.; Wu, S. *Microchim. Acta* **2013**, *180*, 453−460.
(27) Jung, E.; Kim, S.; Kim, Y.; Seo, S. H.; Lee, S. S.; Han, M. S.; Lee, S. *Angew. Chem., Int. Ed.* **2011**, *50*, 4386−4389.
(28) Wei, S.-C.; Hsu, P.-H.; Lee, Y.-F.; Lin, Y.-W.; Huang, C.-C. *ACS Appl. Mater. Interfaces* **2012**, *4*, 2652−2658.
(29) Wang, G.-L.; Zhu, X.-Y.; Dong, Y.-M.; Jiao, H.-J.; Wu, X.-M.; Li, Z.-J. *Talanta* **2013**, *107*, 146−153.
(30) Wang, M.; Wu, Z.; Yang, J.; Wang, G.; Wang, H.; Cai, W. *Nanoscale* **2012**, *4*, 4087−4090.
(31) Zhang, J.; Xu, X.; Yang, C.; Yang, F.; Yang, X. *Anal. Chem.* **2011**, *83*, 3911−3917.
(32) Li, H.-F.; Xie, C.-G. *J. Lumin.* **2012**, *132*, 30−34.
(33) Zhou, G.; Zhao, C.; Pan, C.; Li, F. *Anal. Methods* **2013**, *5*, 2188−2192.
(34) Pilolli, R.; Palmisano, F.; Cioffi, N. *Anal. Bioanal. Chem.* **2012**, *402*, 601−623.
(35) McLean, J. A.; Stumpo, K. A.; Russell, D. H. *J. Am. Chem. Soc.* **2005**, *127*, 5304−5305.
(36) Chen, S.-J.; Huang, C.-C.; Chang, H.-T. *Talanta* **2010**, *81*, 493−498.
(37) Bogen, K. T.; Brorby, G.; Berman, D. W.; Sheehan, P.; Floyd, M. *Ann. Occup. Hyg.* **2002**, *55*, 485−494.
(38) Myagkova, N. V.; Rakhmonberdiev, G. R.; Sagdieva, Z. G.; Sidikov, A. S. *Chem. Nat. Compd.* **1997**, *33*, 76−79.
(39) Rumyantseva, Yu. I.; Zhbankov, R. G. *J. Appl. Spectrosc.* **1985**, *42*, 187−192.
(40) Sidikov, A. S.; Yusupkhodzhaeva, E. N.; Rakhmanberdiev, G. R.; Arslanov, Sh. S. *Chem. Nat. Compd.* **1999**, *35*, 668−670.
(41) Chen, A.; Shi, Z.; Bizzotto, D.; Lipkowski, J.; Pettinger, B.; Bilger, C. *J. Electroanal. Chem.* **1999**, *467*, 342−353.
(42) Werner, D.; Hashimoto, S. *J. Phys. Chem. C* **2011**, *115*, 5063−5072.
(43) Newhouse, R. J.; Wang, H.; Hensel, J. K.; Wheeler, D. A.; Zou, S.; Zhang, J. Z. *J. Phys. Chem. Lett.* **2011**, *2*, 228−235.
(44) Werner, D.; Furube, A.; Okamoto, T.; Hashimoto, S. *J. Phys. Chem. C* **2011**, *115*, 8503−8512.
(45) King, B. V.; Veryovkin, I. V.; Moore, J. F.; Calaway, W. F.; Pellin, M. J. *Surf. Sci.* **2009**, *603*, 819−825.
(46) Picariello, G.; Romano, R.; Addeo, F. *Anal. Chem.* **2010**, *82*, 5783−5791.
(47) Liu, Y.-C.; Chiang, C.-K.; Chang, H.-T.; Lee, Y.-F.; Huang, C.-C. *Adv. Funct. Mater.* **2011**, *21*, 4448−4455.
(48) Liu, Y.-C.; Chang, H.-T.; Chiang, C.-K.; Huang, C.-C. *ACS Appl. Mater. Interfaces* **2012**, *4*, 5241−5248.
(49) Werner, D.; Hashimoto, S.; Uwada, T. *Langmuir* **2010**, *26*, 9956−9963.
(50) Link, S.; Burda, C.; Nikoobakht, B.; El-Sayed, M. A. *J. Phys. Chem. B* **2000**, *104*, 6152−6163.
(51) Cheng, W.; Dong, S.; Wang, E. *Angew. Chem., Int. Ed.* **2003**, *42*, 449−452.
(52) Caldwell, K. L.; Makhmudov, A.; Ely, E.; Jones, R. L.; Wang, R. Y. *Thyroid* **2011**, *21*, 419−427.
(53) Dasgupta, P. K.; Liu, Y.; Dyke, J. V. *Environ. Sci. Technol.* **2008**, *42*, 1315−1323.